Synthesis of penta-fold twinned Pd-Au-Pd segmental nanorods for in situ monitoring catalytic reaction

Guangliang Niu[a,1], Fangyan Liu[b,1], Yun Yang[b,*], Yunzhi Fu[a,*], Wei Wang[c,*]

[a] College of Science, Hainan University, Haikou 570228, China
[b] Nanomaterials and Chemistry Key Laboratory, Wenzhou University, Wenzhou, Zhejiang 325027, China
[c] Department of Chemistry and Center for Pharmacy, University of Bergen, 5020 Bergen, Norway

GRAPHICAL ABSTRACT

Pd-Au-Pd segemental nanorods are prepared in a controlled manner and used for in situ minotoring organic reaction.
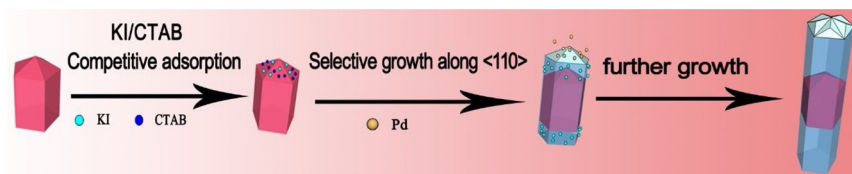
ARTICLE INFO

ABSTRACT

Multimetallic nanomaterials have many applications. The controlled synthesis of multimetallic nanomaterials is highly desired. We report a study on using penta-fold twinned (PFT) Au nanorods (NRs) as seeds to synthesize PFT Pd-Au-Pd segmental NRs. The results show that the different crystal structures of seeds, I⁻ and cetyl-trimethylammonium bromide (CTAB) significantly affect the deposition of Pd on seeds surface. The PFT Pd-Au-Pd segmental NRs showed excellent surface-enhanced Raman scattering (SERS) performance and improved catalytic activity. Our research is of great significance for the synthesis of similar nanostructures, and we also shown that PFT Pd-Au-Pd segmental NRs might have potential applications in studying the process of organic reaction.

1. Introduction

Noble nanostructures have attracted much interest during the past several decades because of their vitally promising applications in plasmonic, catalysis, sensing, bioimaging, photothermal therapy, surface-enhanced Raman scattering, and etc. [1–8]. However, properties of noble nanostructures are highly dependent on the particle size, its morphology, composition, and structure [9–16]. Therefore, synthetic methods for nanoparticles with precise control of their morphology and structure are in demand. Seeded growth is one of the commonly used methods and very effective [17–20]. In the seeded growth, the decisive

factors to achieve a designed morphology contain growth kinetics, thermodynamics, capping agents, lattice mismatch, seed structure, and etc [21–36]. Growth kinetics has a great influence on the growth of the product, so its adjustment can greatly change the shape of the product [21,22]. Thermodynamics mainly affects the surface free energy of the product. In general, the growth often happens on three low index facets, (111), (100), (110) [22,37]. The blocking agent generally adheres to some certain facets to promote preferential growth along a given direction [25,27]. According to a related report, a lattice mismatch between the two metals can be used to effectively induce the formation of twin facets in the seeds, allowing them to grow into anisotropically

shaped metal nanostructures at a remarkable high yield [28]. During the growth of the seed. The generally accepted theory at present is that a small lattice mismatch can promote homogeneous growth in which the whole seed surface acts as a nucleation site and a large lattice mismatch can promote heterogeneous growth in which growth occurs only on part of the seed surface [38–45]. Among these factors, the role of seeds is always crucial, and nanostructures generated by the method are often with the same crystalline structure as the seed itself [2,12]. The formation of Au core-Pd shell nanoparticles (NPs) under kinetically and thermodynamically controlled reaction conditions has been studied previously. By controlling the reaction temperatures, the growth of Au@Pd core-shell NPs can switches from kinetically to thermo-dynamically controlled growth [46]. In practice, The process of seeded growth is affected by above all of the factors, and the dominant factor is not clear under different conditions. Therefore, the coupling among the correlative factors should be synthetically considered.

Multimetallic nanostructures often have better performances comparing to monometallic counterparts due to the synergistic effect of various components and the formation of heterogeneous interface. [2–5,8,47,48], For example, the Ag-Pt nanostructures enhanced the catalytic performance of Pt and reduced the usage of Pt by the synergistic effect of Ag and Pt greatly [49,50]. The Ag/Au alloy nano-spheres combine the excellent plasmonic performance of Ag and the excellent stability of Au, which provides the possibility in the application of many high-performance, long-life plasma materials, especially for those concerning corrosive materials [51,52]. The Au-Pd bimetallic nanostructures have the catalytic properties of both Au and Pd in addition to the property of surface plasma for Au, which enhances its general catalytic performance [48,53]. Among different multimetallic systems, Au-Pd bimetallic nanostructures have received enormous attention as they can be widely used as a highly efficient catalyst [54–59].

Many applications of Au-Pd nanocrystals also showed the correlation between morphology and its properties [54–63]. For example, Au nanocubes were used as structure-directing cores to prepare Au–Pd core-shell nanocrystals with tetrahexahedral, concave octahedral, and octahedral shapes. Au–Pd tetrahexahedral nanocrystals exhibit the best electrocatalytic activity [54]. Therefore, the controlled synthesis of Au-Pd nanostructures has been a very interesting subject. Zheng and co-workers reported a synthetic study on Au–Pd bimetallic nanodendrites with homogeneous alloy structure and well-defined morphology. In the presence of triblock copolymer P123, ascorbic acid reduces the metal precursors, Au and Pd. Ascorbic acid plays a vital role in inducing the adhesion of primary particles to dendritic morphology [60]. By seed-mediated synthetic method with co-reduction, Skrabalak and co-workers synthesized Au-Pd octopods and concave Au@Pd nanocrystals using ascorbic acid as the reducing agent and CTAB as the stabilizing agent. Furthermore, they provided an insight into the mechanism for the architectural formation of the nanostructures [62,63]. Given the complementary synergy of binary Au-Pd nanocrystals in catalytic performance and difficulty in synthesis, there remains a challenge in inaccurate control of morphology.

PFT nanostructure has an important position in nanomaterials [3,38,40,61,64–78]. Noble metallic nanocatalysts with PFT structures exhibit outstanding SERS performance and high selectivity in some chemical reactions [2,79]. Usually, observed PFT nanostructures are NR, nanobipyramid (NBP), nanowires, decahedron and icosahe-dron.38,40,61,64–70] As high-profile stars, PFT NRs, bipyramid and decahedra have received widespread attention [68–76]. PFT NBP and NR are structurally similar to decahedrons. By seeded growth, many scientists used decahedrons as seeds to prepare PFT NRs and NBPs [68–75]. For instance, PFT Au NR could be synthesized by Au decahedrons as seeds in the presence of silver ions by a systematic over-growth.38 Kitaev et al. reported the synthesis of monodisperse size-controlled PFT Ag NRs by thermal regrowth of Ag decahedrons in aqueous solution at 95 °C, using citrate as a reducing agent [64,80]. Seeded growth as a wide applied method can be used to synthesize both single-component PFT nanostructures and bimetallic segmental PFT NRs.61,65,656667686970] [81,82], Teranishi and co-workers used Au decahedra and synthesized high-quality Au@Ag heterogeneous NRs with PFT structure [81]. Using Au decahedra as seeds, our group also synthesized Ag–Au–Ag and PFT Pd-Au-Pd segmental NRs via kinetics-controlled growth [5,61]. Wang et al. demonstrated the preparation of high-aspect-ratio Ag NRs based on Au NBP-directed Ag overgrowth [3]. Our group synthesized PFT Au@Pd nanobipyramids (NBs) with stepped (100) facets through growing Pd on Au decahedral NPs in the polyol. Furthermore, we proved that Br- is a key factor in the growth of Au @ Pd NBs.82]

As mentioned above, the preparation of Au-Pd bimetallic nanos-tructures with regular morphology is still a difficult task. Studying the growth of Pd on different Au seeds is very important for synthesizing various metal heterostructures and revealing the growth rules of such structures. Herein, we used Au NRs with a PFT structure as seeds and CTAB as a capping agent to synthesize PFT Pd-Au-Pd segmental NRs. Meanwhile, the directional growth of Pd on the surface of Au crystals was systematically studied using single crystal Au NRs as seeds.

2. Experimental section

Silver nitrate ($AgNO_3$), potassium iodide (KI), chloroauric acid ($HAuCl_4$), diethylene glycol (DEG), and PDDA (MW = 400,000–500000, 20 wt % in H_2O) were purchased from Sigma-Aldrich. CTAB, ascorbic acid (AA), formic acid, and palladium chloride ($PdCl_2$) were purchased from Aladdin reagent. All chemicals were used as received. Deionized water (18.2 MΩ cm) was generated by the Milli-Q Academic water purification system (Millipore Corp, Billerica, MA, USA) and used in all experiments.

2.1. Preparations of PFT Au NRs

In a typical preparation, 75 μL PDDA was added to 10 mL DEG under magnetic stirring (500 rpm), and then 13 μL $HAuCl_4$ (0.48 M) aqueous solution was introduced, Keeping stirring until the yellow homogeneous solution had formed. Firstly, 4 mg $AgNO_3$ was dissolved in 1 mL DEG and sonicated for 2 min until $AgNO_3$ was completely dissolved. Then, 75 μL of this solution was added to the yellow homogeneous solution, the mixture was stirred for another 3 min. The resulting solution was placed into an oil bath to promote the reduction of Au (III) to Au. After 30 min, a purple-red colloid formed, and then the reaction liquid was removed from the oil bath and slowly cooled down to room temperature. The size of Au nanocrystals can be adjusted by adjusting the reaction temperature and reaction time.

To purify products for characterization, excess DEG, PDDA, and other impurities needed to be removed. 9 mL of water was added to 1 ml of the above sample and then the mixture was centrifuged (12 000 rpm). The precipitates were dispersed in 9 mL of water and precipitated again by centrifuge. The purifying procedure was repeated three times, the precipitate was collected and dissolved in 0.5 mL water for future use.

2.2. Synthesis of PFT Pd-Au-Pd segmental NRs using PFT Au NRs as seeds

A slightly modified method was used to synthesize of PFT Pd-Au-Pd segmental NRs [61]. 1 mL of purified PFT Au NRs was mixed with 2.5 mL of CTAB aqueous solution (0.1 M). 0.12 mL of H_2PdCl_4 (0.01 M), 0.06 mL of KI (0.04 M), and 0.17 mL of AA (0.02 M) were added to the above solution individually. The solution volume was kept to 5 mL in each preparation. Then all mixtures were stirred variously for 5 min and then put into a 90 °C water bath. After about 30 min, and the solutions were cooled down to room temperature. The purification of PFT Pd-Au-Pd segmental NRs was similar to that of PFT Au NRs, except for the centrifuging speed (2000 rpm).

2.3. In situ monitoring organic reaction with SERS

To monitor the catalytic reaction by SERS, first, a self-assembled monolayer (SAM) of p-nitrothiophenol (p-NTP) was adsorbed on the surface of metal nanoparticles. In a typical reaction, 0.5 mL of an aqueous dispersion of metal nanoparticles was mixed into 100 μL of ethanolic solution of 10 mM p-NTP overnight to form a saturated SAM on the surface of the nanoparticles. The products were collected with a centrifuge and then 0.01 ml of nice-cold NaBH₄ solution(60 mM). Subsequently, the mixture containing NaBH₄, p-NTP, and NRs (catalyst) was transferred to a special quartz cell for SERS investigation.

2.4. Characterization

For transmission electron microscopy (TEM), high-resolution transmission electron microscopy (HRTEM), energy-dispersive spectroscopy (EDS), high-angle annular dark-field (HAADF), and scanning transmission electron microscopy EDS (STEM-EDS) characterizations, the purified colloid was deposited on copper grids coated by a carbon membrane and dried at 80 °C. TEM was performed with a 200 kV JEOL 2100 F with an attached EDS and STEM detector. The high-resolution SEM images were obtained with FEI Helios nanolab 600i. The UV–vis spectra of colloid nanostructures were recorded with a Shimadzu 2450 UV–vis spectrophotometer at room temperature. Raman measurement was taken by RENISHAW microRaman system at room temperature (633 nm Ar + laser line excitation, 5 mW).

3. Results and discussion

In previous studies, we have demonstrated the selective growth of Au or Ag on Au seeds to respectively obtain Au NBPs and Ag-Au-Ag NRs with PFT nanostructures by adjusting the growth kinetics [5,67]. Due to the difficulty of growing Pd on the Au surface, it remains a challenge to prepare Pd-Au-Pd segmental NRs with PFT nanostructures under the same conditions. Many previous reports have demonstrated that halide ions preferentially bind to the {100} facets of various metals, which inhibits the growth of the {100} facets [82–84]. Zheng and co-workers prepared Pd Nanowires and NRs with PFT structure in the presence of poly (vinylpyrrolidone) and I⁻ [40]. Therefore, we speculated that I⁻ could be used to assist in the synthesis of PFT Pd-Au-Pd segmental NRs. Using Au decahedra as seed and I- as growth modifiers, our group have successfully prepared high-quality PFT Pd-Au-Pd segmental NRs, and it was proven that the competitive binding (or adsorption) of CTAB and I⁻ in the surface of Au NRs seeds is important in the whole growth process [61]. After a comprehensive study on optimizing the experimental conditions, we used Au NRs with a PFT structure as seeds (Fig. S1) to synthesize PFT Pd-Au-Pd segmental NRs. It was found that the selective growth of Pd atoms along the < 110 > direction of Au NRs could be realized and segmental Pd-Au-Pd NRs were successfully prepared (Fig. 1A–D).

TEM and STEM-EDS were used to further investigate the structure of the samples. The TEM and HRTEM images of PFT Pd-Au-Pd segmental NRs are shown in Fig. 2A–D. In comparison to HAADF images, the contrast of ordinary TEM images follows the inverse law of atomic number because more transmitted electrons are scattered for metals with a higher atomic number. Therefore, the part of Au NR is darker than the Pd segment in the TEM image. The TEM image also shows that the lateral length of Pd–Au–Pd NRs is almost equal to that of Au NRs, indicating that the growth only occurred preferentially only along < 110 > (Fig. 2 A–C). The transverse and longitudinal length distributions of PFT Au NRs and PFT Pd-Au-Pd segmental NRs are shown in Figs. S2 and S3, respectively. Pd-Au-Pd NRs have typical PFT features and the fast Fourier transform (FFT) pattern also demonstrates this (Fig. 2C), which further confirms that Pd atoms grow along < 110 > of the Au NRs. The lattice spacing of adjacent planes is 0.0238 nm and can be attributed to Pd(111) (Fig. 2D).

STEM-EDS technology was used to analyze the elemental distribution of Pd–Au–Pd NRs and obtain further evidence of the segmental structure (Fig. 3 A–D). In Figs. 3B and C, the elemental distribution of Pd and Au demonstrates the products are segmental Pd-Au-Pd NRs, which is consistent with above TEM, HRTEM, and HAADF observations (Figs. 1 and 2). The lineal profile of composition also gives the same conclusion (Fig. 3D).

Segmented multi-metal NRs have attracted wide attention due to the applications [2,3,8]. However, the synthesis of segmented metal NRs with precisely controlled composition and morphology is still very challenging. The AAO template can be used to selectively synthesize segmented NRs by selective electrodeposition, but the yield is very low [85–87]. Through the seeded growth, we have prepared PFT Pd-Au-Pd segmental NRs (Fig. 4A, B). The SEM images demonstrate that the synthesis has a high yield.

To investigate how PFT Au NRs affects the deposition of Pd atoms on Au NRs, single-crystalline Au NRs were also used as seeds in a controlled experiment. The result shows that Au@Pd nanocuboids were formed and no Pd-Au-Pd segmental NRs were observed (Figure S4, S5). Distinctively, the crystalline feature of Au NRs is extremely important for the growth of PFT Pd-Au-Pd segmental NRs. In another set of experiments, we also performed the synthesis without seeds. When no seeds were introduced and other conditions remained unchanged, monodispersed Pd nanocubes were obtained (Figure S6). This further demonstrates the importance of PFT Au NRs seeds in the growth of PFT Pd-Au-Pd segmental NRs.

We also studied the structure change with CTAB. When 0.01 M CTAB was introduced, most of the products were single crystal Pd nanocubes, and only a small part of PFT Pd-Au-Pd segmental NRs were produced (Fig. 5A). This indicates that the self-nucleation of Pd is dominant at low concentrations of CTAB, and the selective deposition of Pd atoms on Au NRs is weak. Using the CTAB concentration of 0.02 M, the amount of PFT Pd-Au-Pd segmental NRs increased slightly. When the concentration of CTAB was increased to 0.05 M, the product mainly contains the PFT Pd-Au-Pd segmental NRs. However, there is still a small amount of single-crystal Pd nanocubes. When increasing the CTAB concentration to 0.1 M, the PFT Pd-Au-Pd segmental NRs yield the desired structure. Further increasing the concentration of CTAB had no significant effect on the crystal structure of the product. Therefore, the high concentration of CTAB promoted the preferential growth of Pd atoms on Au NRs.

Growth kinetics can affect morphology and structure of products [21–23]. In the experiment, the concentration of precursors could be used to control the growth kinetics [21]. Based on our previous study, the concentration of Pd precursor has little effect on the product PFT segmental structure [61]. By reducing the concentration of Pd precursors, we found that the Pd NRs was significantly shortened, and the segmental structure of Pd-Au-Pd NRs was still formed (Fig. 6A-D).

3.1. Possible mechanism

In our system, three factors are crucial, which are the seeds, I⁻ and CTAB. The seeds have a typical PFT structure, which tends to induce the growth of products with the same structure. The single-crystal Au NRs induced to form the core-shell Au@Pd structures (Figure S4), indicating that seeds are critical in the synthesis. Here we propose a possible mechanism for the seed growth as illustrated in Fig. 7.

Many reports have shown that I⁻ can absorb on the Pd(100) crystal facets, and thereby reduce the surface energy of (100) [40,76]. The same results was observed in our experiments. Without the seeds, (100)-bounded Pd nanocubes were obtained (Figure S6), confirming that I⁻ indeed absorb on (100). The seeded growth is closely related to the surface energy of crystal facets, and the growth tends to cover high-energy facets first. The PFT Pd-Au-Pd segmental NRs have two crystal facets, (111) and (100), and the surface energy of (100) crystal facets is higher than that of (111). In theory, growth should occur on (100)
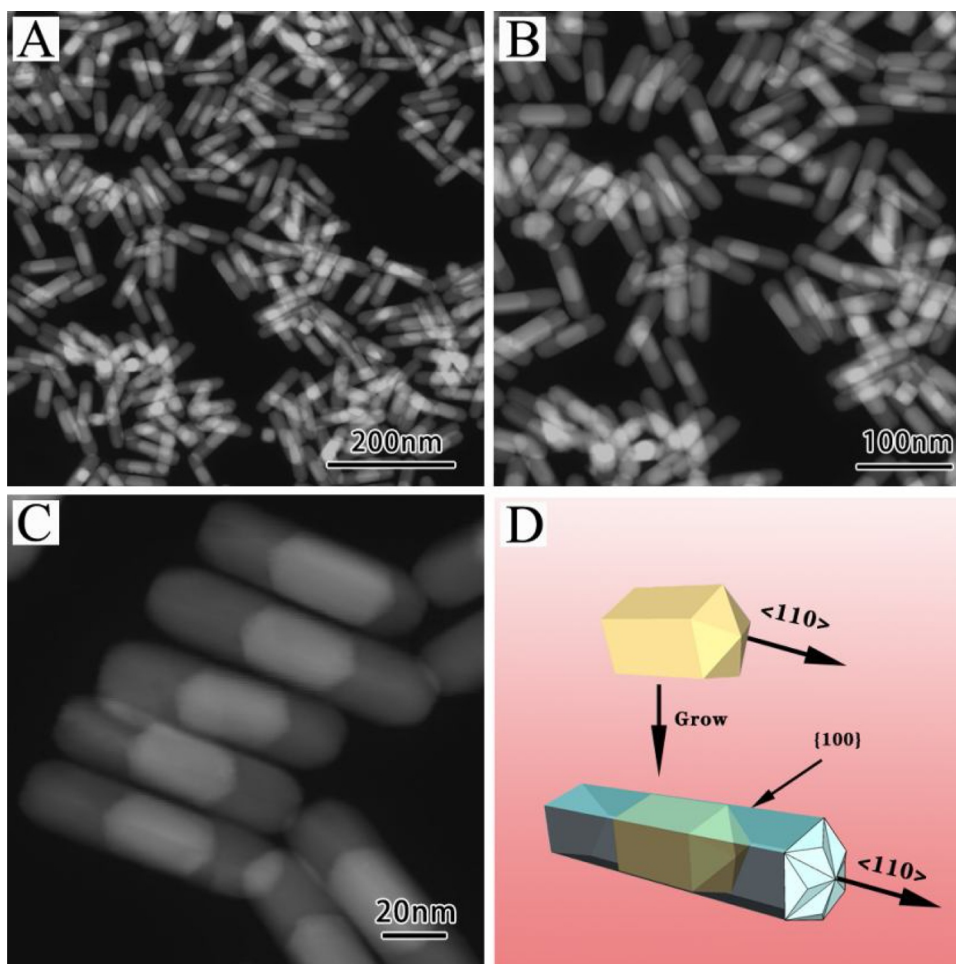
Fig. 1. (A, B, C) HAADF images of PFT Pd-Au-Pd segmental NRs prepared in a standard procedure. (D) Schematic illustration of growing PFT Pd-Au-Pd segmental NRs.
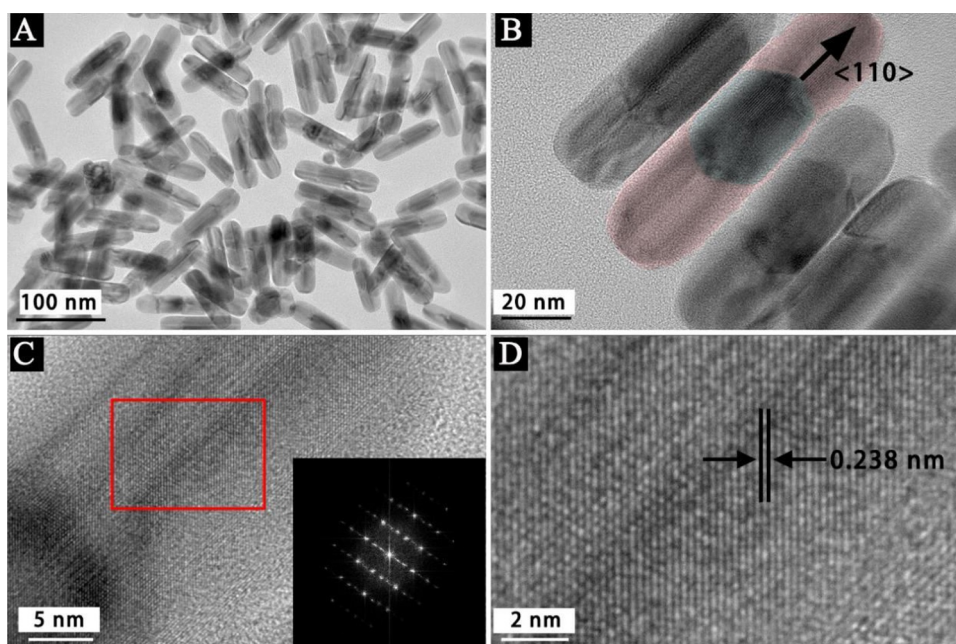

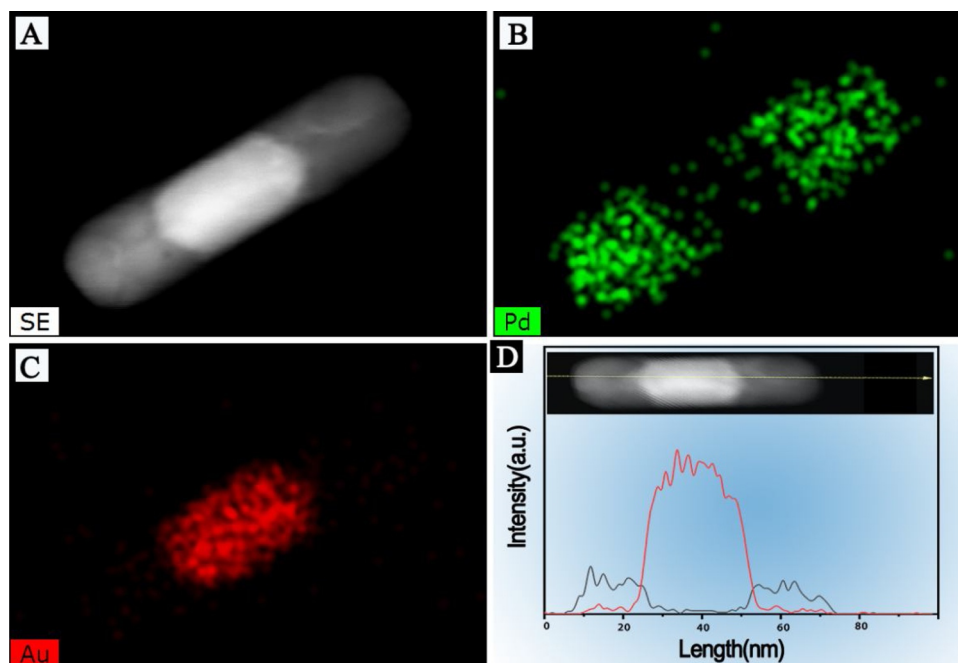**Fig. 2.** (A–D) TEM and HRTEM images of PFT Pd-Au-Pd segmental NRs.

Fig. 3. (A–C) HAADF image and elemental mapping patterns of a complete PFT Pd-Au-Pd segmental NRs. (D) Cross-sectional compositional line profiles of one P PFT Pd-Au-Pd segmental NRs.
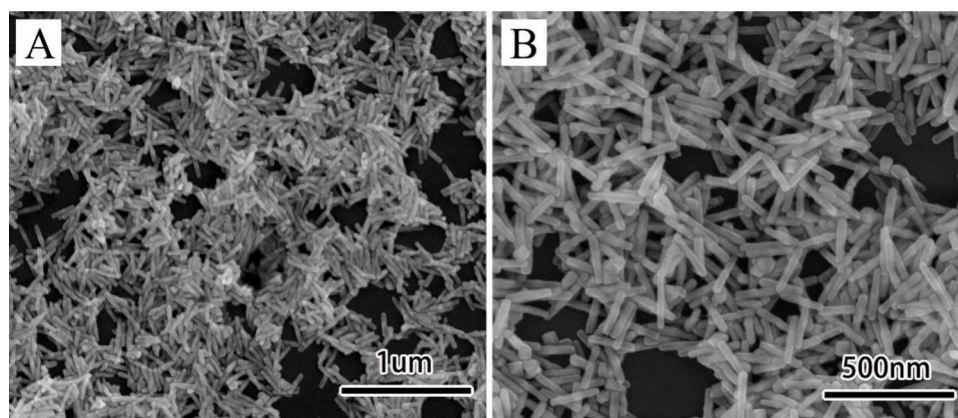

Fig. 4. (A, B) SEM images of the PFT Pd-Au-Pd segmental NRs samples.

crystal facets. However, the selective adsorption of I$^-$ leads to a reduction in the surface energy of the (100) crystal facets, which promotes the growth on the (111) crystal facets along the < 110 > direction.

CTAB has two effects in the reaction system. One is as capping agent to stabilize particles from gathering. The other is to compete with I$^-$ on the adsorption to (111) facet [61]. I- has a stronger affinity with metal atoms than Br$^-$ [76,82]. The adsorption of I$^-$ can greatly reduce the surface energy. The introduction of CTAB can reduce the absorption of I$^-$ due to the competitive effect and increase surface activity. Therefore, the deposition and growth of Pd atoms on the (111) are facilitated. If the CTAB concentration is extremely low, a large amount of I$^-$ is absorbed on both (111) crystal facets and the (100) crystal facets, resulting in the low surface activity of seed. As a result, the deposition of Pd atoms on the seed surface is not preferred and self-nucleation occurs (Fig. 5A, B), which causes the formation of pure Pd nanoparticles. As the concentration of CTAB increases, more CTAB molecules were adsorbed on the (111) facet of the Au seeds, replacing part of the adsorbed I$^-$ on the surface of the Au seed. The surface activity of the seeds increases, promoting the nucleation of Pd atoms on the seed surface.

3.2. In situ monitoring organic reaction with SERS

Pd-based NPs are often excellent high-performance catalysts.31,72 When Pd NPs deposited on the Au NRs, they could be multifunctional and thus useful for catalytic reactions. To gain insight into the catalytic activity of PFT Pd-Au-Pd segmental NRs, we selected the conversion reaction of 4-nitrothiophenol (4-NTP) to 4-aminothiophenol (4-ATP) as the model reaction, which has been widely used to evaluate the catalytic activity of noble nanomaterials [88,89]. 4-NTP was adsorbed on the surface of PFT Pd-Au -Pd segmental NRs through thiol groups to form a self-assembled molecular layer. Then the Raman signal of the adsorbed molecules on the surface of the nanoparticles was collected and analyzed to study the reaction kinetics of the reactant (4-NTP) or the product (4-ATP). 4-NTP accumulated on the catalyst surface, avoiding the adsorption and desorption of reactants and products on the catalyst surface, which is beneficial to our research. The characteristic vibrational bands of 4-NTP in the Raman spectrum are 1330 cm^{-1} and 1570 cm^{-1}, which are ON=−O symmetric stretching and phenyl ring stretching modes, respectively (Fig. 8B). When NaBH$_4$ was added, the peaks at 1330 cm^{-1} and 1570 cm^{-1} gradually weakened. However, a new peak appeared at about 1593 cm^{-1}, which was
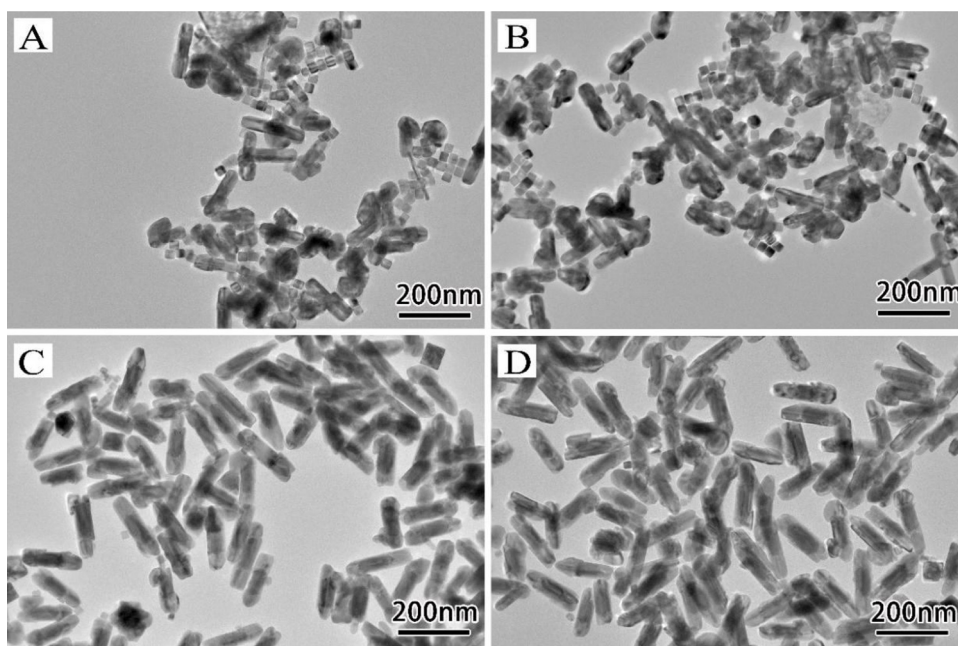
Fig. 5. TEM images of products prepared using different concentrations of CTAB : (A) 0.01 M; (B) 0.02 M; (C) 0.05 M; (D) 0.1 M.
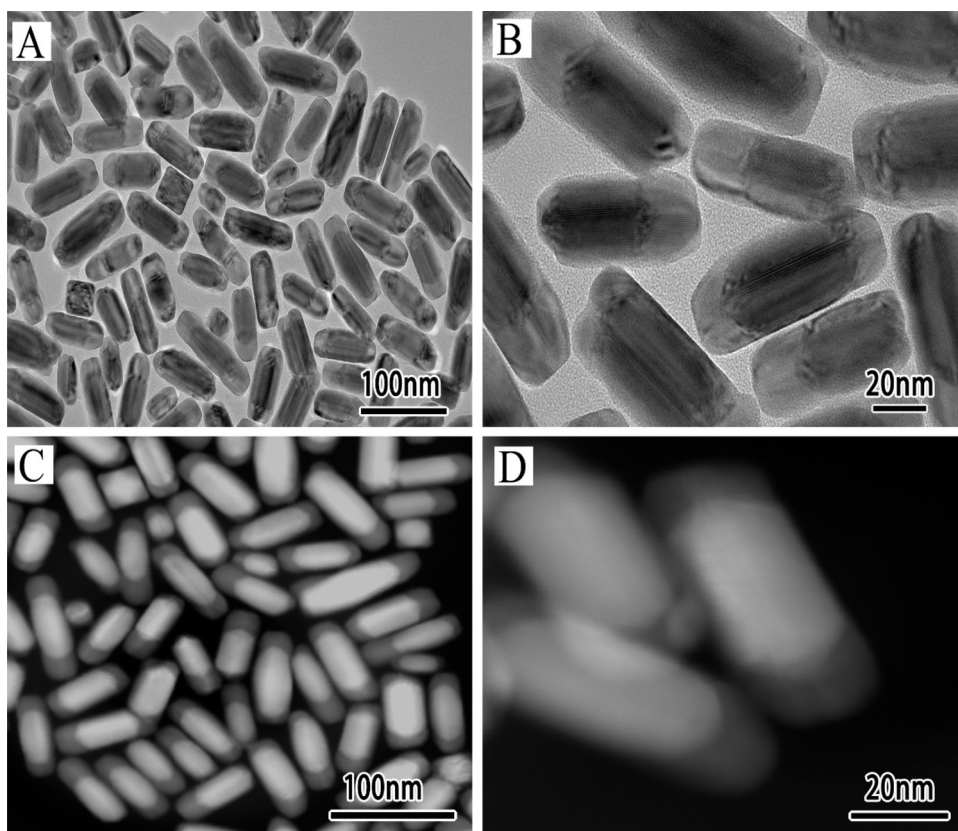

Fig. 6. (A, B) TEM images of PFT Pd-Au-Pd segmental NRs with half amount of Pd. (C, D) HAADF images of PFT Pd-Au-Pd segmental NRs prepared with half amount of Pd.

assigned to the phenyl ring of 4-ATP. To verify that our PFT Pd-Au-Pd segmental NRs have the good catalytic ability, we used the same molar amount of PFT Au NRs as a control experiment. When we used PFT Pd-Au-Pd segmental NRs as a catalyst, the Raman characteristic peak of the 4-ATP benzene ring is detected at 15 min, and when the reaction reached 35 min, the peaks at 1330 cm^{-1} and 1570 cm^{-1} have

completely disappeared, and the characteristic peak of 4-ATP was obvious. At 50 min, there is still no change, which means that 4-NTP has been completely converted to 4-ATP in 35 min. Using the same amount of PFT Au NRs as a catalyst, the characteristic peak of 4-NTP is still obvious when the reaction continues to 60 min, and the characteristic peak of 4-ATP does not show a trend (Fig. 8A). It means that there is
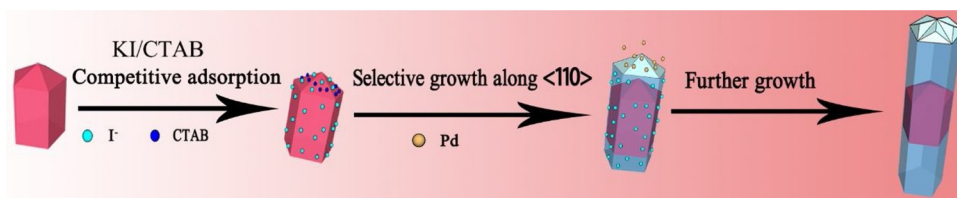
Fig. 7. an illustration of the growth mechanism of the PFT Pd-Au-Pd segmental NRs.
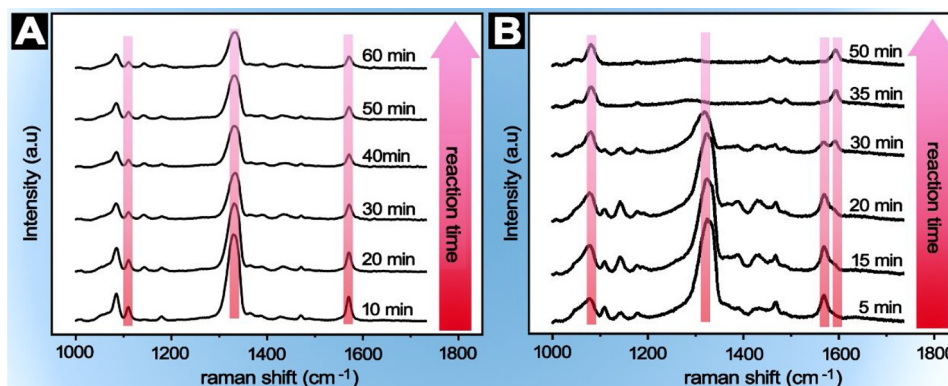

Fig. 8. (A) Raman spectra using PFT Au NRs as substrate materials. (B) Raman spectra using PFT Pd-Au-Pd segmental NRs as substrate materials.

still no 4-ATP formation after 1 h of reaction. By using the same amount of PFT Pd-Au-Pd segmental NRs and Au NRs to catalyze the conversion of 4-NTP to 4-ATP and performing SERS detection analysis of in-situ Raman, it was proved that PFT Pd-Au-Pd segmental NRs with Pd surface properties have excellent catalytic performance.

4. Conclusion

We have demonstrated that PFT Pd-Au-Pd segmental NRs can be synthesized through growing Pd on PFT Au NRs. Our results show that CTAB, I⁻ and seed are three crucial factors in the growth of PFT Pd-Au-Pd NRs. PFT Au NRs seeds act as templates inducing the formation of nanocrystal with the same structure as the seeds. The selective adsorption of I- reduces the surface energy of the (100) crystal facets, and thereby promotes the growth of Pd atoms along the < 110 > direction. CTAB can reduce the adsorption of I- on the (111) facets and increase the activity, which facilitates the deposition of Pd atoms. In situ monitoring organic reaction with SERS, the prepared PFT Pd-Au-Pd segmental NRs showed better catalytic performance than PFT Au NRs due to the catalytic activity of Pd. Our research is of great significance for the precise control of the composition and structure of multimetallic nanostructures. Moreover, the prepared PFT Pd-Au-Pd Segmental NRs also have potential applications in studying the process of organic reaction.

CRediT authorship contribution statement

Guangliang Niu: Investigation, Writing - original draft. **Fangyan Liu:** Methodology, Investigation. **Yun Yang:** Conceptualization, Funding acquisition, Project administration, Writing - review & editing. **Yunzhi Fu:** Supervision. **Wei Wang:** Conceptualization, Investigation, Supervision, Writing - original draft, Writing - review & editing.

Declaration of Competing Interest

The authors reported no declarations of interest.

Acknowledgment

Appendix A. Supplementary data

Supplementary material related to this article can be found, in the online version, at doi:https://doi.org/10.1016/j.colsurfa.2020.125490.

References

[1] K.-K. Liu, S. Tadepalli, L. Tian, S. Singamaneni, Size-dependent surface enhanced Raman scattering activity of plasmonic nanorattles, Chem. Mater. 27 (2015) 5261–5270.
[2] P. Singh, T.A.F. König, A. Jaiswal, NIR-active plasmonic gold nanocapsules synthesized using thermally induced seed twinning for surface-enhanced Raman scattering applications, ACS Appl. Mater. Interfaces 10 (2018) 39380–39390.
[3] X. Zhuo, X. Zhu, Q. Li, Z. Yang, J. Wang, Gold nanobipyramid-directed growth of length-variable silver nanorods with multipolar plasmon resonances, ACS Nano 9 (2015) 7523–7535.
[4] L. Zhang, et al., Gold nanoframes by nonepitaxial growth of Au on AgI nanocrystals for surface-enhanced Raman spectroscopy, Nano Lett. 15 (2015) 4448–4454.
[5] Y. Yang, et al., Controlled growth of Ag/Au bimetallic nanorods through kinetics control, Chem. Mater. 25 (2013) 34–41.
[6] L. Scarabelli, M. Coronado-Puchau, J.J. Giner-Casares, J. Langer, L.M. Liz-Marzán, Monodisperse gold nanotriangles: size control, large-scale self-assembly, and performance in surface-enhanced Raman scattering, ACS Nano 8 (2014) 5833–5842.
[7] P. Singh, S. Roy, A. Jaiswal, Cubic gold nanorattles with a solid octahedral core and porous shell as efficient catalyst: immobilization and kinetic analysis, J. Phys. Chem. C 121 (2017) 22914–22925.
[8] D. Seo, C.I. Yoo, J. Jung, H. Song, Ag−Au−Ag heterometallic nanorods formed through directed anisotropic growth, J. Am. Chem. Soc. 130 (2008) 2940–2941.
[9] J. Mao, Y. Chen, J. Pei, D. Wang, Y. Li, Pt–M (M = Cu, Fe, Zn, etc.) bimetallic nanomaterials with abundant surface defects and robust catalytic properties, Chem. Commun. 52 (2016) 5985–5988.
[10] W. Niu, Y.A.A. Chua, W. Zhang, H. Huang, X. Lu, Highly symmetric gold nanostars: crystallographic control and surface-enhanced Raman scattering property, J. Am. Chem. Soc. 137 (2015) 10460–10463.
[11] T. Miao, et al., Correlation of surface Ag content in AgPd shells of ultrasmall core–shell Au@AgPd nanoparticles with enhanced electrocatalytic performance for ethanol oxidation, J. Phys. Chem. C 119 (2015) 18434–18443.
[12] S. Lee, et al., Synthesis and optical property characterization of elongated AuPt and Pt@Au metal nanoframes, Nanoscale 8 (2016) 4491–4494.
[13] Y.-C. Tsao, S. Rej, C.-Y. Chiu, M.H. Huang, Aqueous phase synthesis of Au–Ag core–shell nanocrystals with tunable shapes and their optical and catalytic properties, J. Am. Chem. Soc. 136 (2014) 396–404.
[14] Y. Zhou, H.C. Zeng, Transition-metal-ions-induced coalescence: stitching Au nanoclusters into tubular Au-based nanocomposites, Small 12 (2016) 2652–2664.
[15] X. Liang, et al., Au decahedra with High yield for the improved synthesis of Au nanobipyramids, Colloids Surf. Physicochem. Eng. Asp. 597 (2020) 124749.

[16] L. Chen, et al., Design of Cu2O-Au composite microstructures for surface-enhanced Raman scattering study, Colloids Surf. Physicochem. Eng. Asp. 507 (2016) 96–102.

[17] W. Wang, et al., Seed-mediated growth of Au nanorings with size control on Pd ultrathin nanosheets and their tunable surface plasmonic properties, Nanoscale 8 (2016) 3704–3710.

[18] M.L. Personick, C.A. Mirkin, Making sense of the mayhem behind shape control in the synthesis of gold nanoparticles, J. Am. Chem. Soc. 135 (2013) 18238–18247.

[19] S.E. Lohse, C.J. Murphy, The quest for shape control: a history of gold nanorod synthesis, Chem. Mater. 25 (2013) 1250–1261.

[20] A. Sánchez-Iglesias, et al., High-yield seeded growth of monodisperse pentatwinned gold nanoparticles through thermally induced seed twinning, J. Am. Chem. Soc. 139 (2017) 107–110.

[21] Y. Wang, J. He, C. Liu, W.H. Chong, H. Chen, Thermodynamics versus kinetics in nanosynthesis, Angew. Chem. Int. Ed. 54 (2015) 2022–2051.

[22] K.D. Gilroy, R.A. Hughes, S. Neretina, Kinetically controlled nucleation of silver on surfactant-free gold seeds, J. Am. Chem. Soc. 136 (2014) 15337–15345.

[23] Y. Xia, X. Xia, H.-C. Peng, Shape-controlled synthesis of colloidal metal nanocrystals: thermodynamic versus kinetic products, J. Am. Chem. Soc. 137 (2015) 7947–7966.

[24] J. Yoon, et al., High yield synthesis of catalytically active five-fold twinned Pt nanorods from a surfactant-ligated precursor, Chem. Commun. 49 (2012) 573–575.

[25] F. Wang, et al., Heteroepitaxial growth of high-index-faceted palladium nanoshells and their catalytic performance, J. Am. Chem. Soc. 133 (2011) 1106–1111.

[26] M.N. O'Brien, M.R. Jones, K.L. Kohlstedt, G.C. Schatz, C.A. Mirkin, Uniform circular disks with synthetically tailorable diameters: two-dimensional nanoparticles for plasmonics, Nano Lett. 15 (2015) 1012–1017.

[27] X. Ye, C. Zheng, J. Chen, Y. Gao, C.B. Murray, Using binary surfactant mixtures to simultaneously improve the dimensional tunability and monodispersity in the seeded growth of gold nanorods, Nano Lett. 13 (2013) 765–771.

[28] Z. Wang, et al., Lattice-mismatch-Induced twinning for seeded growth of anisotropic nanostructures, ACS Nano 9 (2015) 3307–3313.

[29] R.G. Weiner, M.R. Kunz, S.E. Skrabalak, Seeding a new kind of garden: synthesis of architecturally defined multimetallic nanostructures by seed-mediated co-reduction, Acc. Chem. Res. 48 (2015) 2688–2695.

[30] X. Li, et al., The unusual effect of AgNO 3 on the growth of Au nanostructures and their catalytic performance, Nanoscale 5 (2013) 4976–4985.

[31] K. Suwannarat, K. Thongthai, S. Ananta, L. Srisombat, Synthesis of hollow trimetallic Ag/Au/Pd nanoparticles for reduction of 4-nitrophenol, Colloids Surf. Physicochem. Eng. Asp. 540 (2018) 73–80.

[32] B. Lv, Z. Sun, J. Zhang, C. Jing, Multifunctional satellite Fe3O4-Au@TiO2 nanostructure for SERS detection and photo-reduction of Cr(VI), Colloids Surf. Physicochem. Eng. Asp. 513 (2017) 234–240.

[33] C. Gong, Q. Li, H. Zhou, R. Liu, Tiny Au satellites decorated Fe3O4@3-aminophenol-formaldehyde core-shell nanoparticles: easy synthesis and comparison in catalytic reduction for cationic and anionic dyes, Colloids Surf. Physicochem. Eng. Asp. 540 (2018) 67–72.

[34] H. Kobara, K. Nakatsuka, A. Wakisaka, Size-selected synthesis of metal nanoparticles by using electrospray in a liquid medium, Colloids Surf. Physicochem. Eng. Asp. 581 (2019) 123836.

[35] C. Zhao, et al., Shape-selective isolation of Au nanoplates from complex colloidal media by depletion flocculation, Colloids Surf. Physicochem. Eng. Asp. 568 (2019) 216–223.

[36] Z. Slavkova, J. Genova, H. Chamati, M. Koroleva, D. Yancheva, Influence of hydrophobic Au nanoparticles on SOPC lipid model systems, Colloids Surf. Physicochem. Eng. Asp. 125090 (2020), https://doi.org/10.1016/j.colsurfa.2020.125090.

[37] N. Murshid, V. Kitaev, Role of poly(vinylpyrrolidone) (PVP) and other sterically protecting polymers in selective stabilization of {111} and {100} facets in pentagonally twinned silver nanoparticles, Chem. Commun. 50 (2014) 1247–1249.

[38] D. Seo, et al., One-dimensional gold nanostructures through directed anisotropic overgrowth from gold decahedrons, J. Phys. Chem. C 113 (2009) 3449–3454.

[39] F. Wetz, et al., Hybrid co–Au nanorods: controlling Au nucleation and location, Angew. Chem. Int. Ed. 46 (2007) 7079–7081.

[40] X. Huang, N. Zheng, One-Pot, High-Yield Synthesis of 5-Fold Twinned Pd Nanowires and Nanorods, J. Am. Chem. Soc. 131 (2009) 4602–4603.

[41] W. He, et al., Pt-guided formation of Pt−Ag alloy nanoislands on Au nanorods and improved methanol electro-oxidation, J. Phys. Chem. C 113 (2009) 10505–10510.

[42] J. Zhang, Y. Tang, K. Lee, M. Ouyang, Nonepitaxial growth of hybrid core-shell nanostructures with large lattice mismatches, Science 327 (2010) 1634–1638.

[43] H. Yu, et al., Dumbbell-like bifunctional Au−Fe3O4 nanoparticles, Nano Lett. 5 (2005) 379–382.

[44] N.E. Motl, J.F. Bondi, R.E. Schaak, Synthesis of colloidal Au–Cu2S heterodimers via chemically triggered phase segregation of AuCu nanoparticles, Chem. Mater. 24 (2012) 1552–1554.

[45] J. Jung, D. Seo, G. Park, S. Ryu, H. Song, Ag−Au−Ag heterometal nanowires: synthesis, diameter control, and dual transversal modes with diameter dependency, J. Phys. Chem. C 114 (2010) 12529–12534.

[46] S.F. Tan, et al., In situ kinetic and thermodynamic growth control of Au–Pd core–shell nanoparticles, J. Am. Chem. Soc. 140 (2018) 11680–11685.

[47] D. Huo, et al., One-dimensional metal nanostructures: from colloidal syntheses to applications, Chem. Rev. 119 (2019) 8972–9073.

[48] S. Rodal-Cedeira, et al., Plasmonic Au@Pd nanorods with boosted refractive index susceptibility and SERS efficiency: a multifunctional platform for hydrogen sensing and monitoring of catalytic reactions, Chem. Mater. 28 (2016) 9169–9180.

[49] Y. Qu, R. Cheng, Q. Su, X. Duan, Plasmonic enhancements of photocatalytic activity of Pt/n-Si/Ag photodiodes using Au/Ag core/shell nanorods, J. Am. Chem. Soc. 133

(2011) 16730–16733.

[50] S.-C. Lin, C.-S. Hsu, S.-Y. Chiu, T.-Y. Liao, H.M. Chen, Edgeless Ag–Pt bimetallic nanocages: in situ monitor plasmon-induced suppression of hydrogen peroxide formation, J. Am. Chem. Soc. 139 (2017) 2224–2233.

[51] C. Gao, Y. Hu, M. Wang, M. Chi, Y. Yin, Fully alloyed Ag/Au nanospheres: combining the plasmonic property of Ag with the stability of Au, J. Am. Chem. Soc. 136 (2014) 7474–7479.

[52] M. Cao, et al., Fully alloying AuAg nanorods in a photothermal nano-oven: superior plasmonic property and enhanced chemical stability, ACS Omega 3 (2018) 18623–18629.

[53] J. Xu, et al., Biphasic Pd−Au alloy catalyst for low-temperature CO oxidation, J. Am. Chem. Soc. 132 (2010) 10398–10406.

[54] C.-L. Lu, K.S. Prasad, H.-L. Wu, J.A. Ho, M.H. Huang, Au nanocube-directed fabrication of Au−Pd core−shell nanocrystals with tetrahexahedral, concave octahedral, and octahedral structures and their electrocatalytic activity, J. Am. Chem. Soc. 132 (2010) 14546–14553.

[55] J.K. Edwards, et al., Au–Pd supported nanocrystals as catalysts for the direct synthesis of hydrogen peroxide from H2 and O2, Green Chem. 10 (2008) 388–394.

[56] J.K. Edwards, et al., Direct synthesis of hydrogen peroxide from H2 and O2 using TiO2-supported Au–Pd catalysts, J. Catal. 236 (2005) 69–79.

[57] D. Wang, A. Villa, F. Porta, L. Prati, D. Su, Bimetallic gold/palladium catalysts: correlation between nanostructure and synergistic effects, J. Phys. Chem. C 112 (2008) 8617–8622.

[58] S. Marx, A. Baiker, Beneficial interaction of gold and palladium in bimetallic catalysts for the selective oxidation of benzyl alcohol, J. Phys. Chem. C 113 (2009) 6191–6201.

[59] D.I. Enache, et al., Solvent-free oxidation of primary alcohols to aldehydes using Au-Pd/TiO2 catalysts, Science 311 (2006) 362–365.

[60] L. Shi, et al., One-step synthesis of Au–Pd alloy nanodendrites and their catalytic activity, J. Phys. Chem. C 117 (2013) 12526–12536.

[61] L. Xu, et al., Competitive effect in the growth of Pd–Au–Pd segmental nanorods, Chem. Mater. 28 (2016) 7394–7403.

[62] C.J. DeSantis, A.C. Sue, M.M. Bower, S.E. Skrabalak, Seed-mediated co-reduction: a versatile route to architecturally controlled bimetallic nanostructures, ACS Nano 6 (2012) 2617–2628.

[63] C.J. DeSantis, A.A. Peverly, D.G. Peters, S.E. Skrabalak, Octopods versus concave nanocrystals: control of morphology by manipulating the kinetics of seeded growth via Co-reduction, Nano Lett. 11 (2011) 2164–2168.

[64] N. Murshid, D. Keogh, V. Kitaev, Optimized synthetic protocols for preparation of versatile plasmonic platform based on silver nanoparticles with pentagonal symmetries, Part. Part. Syst. Charact. 31 (2014) 178–189.

[65] M.R. Langille, J. Zhang, C.A. Mirkin, Plasmon-mediated synthesis of heterometallic nanorods and icosahedra, Angew. Chem. Int. Ed. 50 (2011) 3543–3547.

[66] X. Zhu, X. Zhuo, Q. Li, Z. Yang, J. Wang, Gold nanobipyramid-supported silver nanostructures with narrow plasmon linewidths and improved chemical stability, Adv. Funct. Mater. 26 (2016) 341–352.

[67] G. Zhou, et al., Growth of Nanobipyramid by using large sized Au decahedra as seeds, ACS Appl. Mater. Interfaces 5 (2013) 13340–13352.

[68] M. Luo, et al., Facile synthesis of Ag nanorods with no plasmon resonance peak in the visible region by using Pd Decahedra of 16 nm in size as seeds, ACS Nano 9 (2015) 10523–10532.

[69] L. Zhang, Q. Chen, X. Wang, Z. Jiang, Nucleation-mediated synthesis and enhanced catalytic properties of Au–Pd bimetallic tripods and bipyramids with twinned structures and high-energy facets, Nanoscale 8 (2016) 2819–2825.

[70] M. Luo, et al., Penta-twinned copper nanorods: facile synthesis via seed-mediated growth and their tunable plasmonic properties, Adv. Funct. Mater. 26 (2016) 1209–1216.

[71] J.-H. Lee, K.J. Gibson, G. Chen, Y. Weizmann, Bipyramid-templated synthesis of monodisperse anisotropic gold nanocrystals, Nat. Commun. 6 (2015) 1–9.

[72] X. Wang, et al., Pd@Pt core–shell concave decahedra: a class of catalysts for the oxygen reduction reaction with enhanced activity and durability, J. Am. Chem. Soc. 137 (2015) 15036–15042.

[73] T. Bian, et al., Epitaxial growth of twinned Au–Pt core–shell star-shaped decahedra as highly durable electrocatalysts, Nano Lett. 15 (2015) 7808–7815.

[74] T. Lv, et al., Controlling the growth of Au on icosahedral seeds of Pd by manipulating the reduction kinetics, J. Phys. Chem. C 120 (2016) 20768–20774.

[75] Q. Shi, et al., Two-dimensional bipyramid plasmonic nanoparticle liquid crystalline superstructure with four distinct orientational packing orders, ACS Nano 10 (2016) 967–976.

[76] Y. Tang, R.E. Edelmann, S. Zou, Length tunable penta-twinned palladium nanorods: seedless synthesis and electrooxidation of formic acid, Nanoscale 6 (2014) 5630–5633.

[77] H. Huang, et al., Five-fold twinned Pd nanorods and their use as templates for the synthesis of bimetallic or hollow nanostructures, ChemNanoMat 1 (2015) 246–252.

[78] F. Cui, et al., Synthesis of ultrathin copper nanowires using tris(trimethylsilyl)silane for high-performance and low-haze transparent conductors, Nano Lett. 15 (2015) 7610–7615.

[79] Y.-H. Chen, H.-H. Hung, M.H. Huang, Seed-mediated synthesis of palladium nanorods and branched nanocrystals and their use as recyclable suzuki coupling reaction catalysts, J. Am. Chem. Soc. 131 (2009) 9114–9121.

[80] B. Pietrobon, M. McEachran, V. Kitaev, Synthesis of size-controlled faceted pentagonal silver nanorods with tunable plasmonic properties and self-assembly of these nanorods, ACS Nano 3 (2009) 21–26.

[81] C. Li, L. Sun, Y. Sun, T. Teranishi, One-pot controllable synthesis of Au@Ag heterogeneous nanorods with highly tunable plasmonic absorption, Chem. Mater. 25 (2013) 2580–2590.

[82] F. Liu, et al., Rational selection of halide ions for synthesizing highly active Au@Pd nanobipyramids, RSC Adv. 7 (2017) 36867–36875.

[83] M. Ho Kim, et al., Maneuvering the growth of silver nanoplates: use of halide ions to promote vertical growth, J. Mater. Chem. C 2 (2014) 6165–6170.

[84] N. Garg, C. Scholl, A. Mohanty, R. Jin, The role of bromide ions in seeding growth of Au nanorods, Langmuir 26 (2010) 10271–10276.

[85] S. Kim, S.K. Kim, S. Park, Bimetallic gold−silver nanorods produce multiple surface plasmon bands, J. Am. Chem. Soc. 131 (2009) 8380–8381.

[86] M.J. Banholzer, L. Qin, J.E. Millstone, K.D. Osberg, C.A. Mirkin, On-wire lithography: synthesis, encoding and biological applications, Nat. Protoc. 4 (2009) 838–848.

[87] S. Kim, K.L. Shuford, H.-M. Bok, S.K. Kim, S. Park, Intraparticle surface plasmon coupling in quasi-one-dimensional nanostructures, Nano Lett. 8 (2008) 800–804.

[88] G. Zheng, L.M. Polavarapu, L. Liz-Marzán, I. Pastoriza-Santos, J. Pérez-Juste, Gold nanoparticle-loaded filter paper: a recyclable dip-catalyst for real-time reaction monitoring by surface enhanced Raman scattering, Chem. Commun. 51 (2015) 4572–4575.

[89] J. Li, J. Liu, Y. Yang, D. Qin, Bifunctional Ag@Pd-Ag nanocubes for highly sensitive monitoring of catalytic reactions by surface-enhanced raman spectroscopy, J. Am. Chem. Soc. 137 (2015) 7039–7042.